VIP Organic Semiconductors Very Important Paper

How to cite: *Angew. Chem. Int. Ed.* **2021**, *60*, 20274–20279
International Edition: doi.org/10.1002/anie.202108224
German Edition: doi.org/10.1002/ange.202108224

High Mobility Organic Lasing Semiconductor with Crystallization-Enhanced Emission for Light-Emitting Transistors

Dan Liu[+], Qing Liao[+], Qian Peng[+], Haikuo Gao, Qi Sun, Jianbo De, Can Gao, Zhagen Miao, Zhengsheng Qin, Jiaxin Yang, Hongbing Fu, Zhigang Shuai, Huanli Dong, and Wenping Hu*

Abstract: *The development of high mobility organic laser semiconductors with strong emission is of great scientific and technical importance, but challenging. Herein, we present a high mobility organic laser semiconductor, 2,7-diphenyl-9H-fluorene (LD-1) showing unique crystallization-enhanced emission guided by elaborately modulating its crystal growth process. The obtained one-dimensional nanowires of LD-1 show outstanding integrated properties including: high absolute photoluminescence quantum yield (PLQY) approaching 80 %, high charge carrier mobility of 0.08 $cm^2 V^{-1} s^{-1}$, Fabry-Perot lasing characters with a low threshold of 86 $\mu J\,cm^{-2}$ and a high-quality factor of ≈2400. Furthermore, electrically induced emission was obtained from an individual LD-1 crystal nanowire-based light-emitting transistor due to the recombination of holes and electrons simultaneously injected into the nanowire, which provides a good platform for the study of electrically pumped organic lasers and other related ultrasmall integrated electrical-driven photonic devices.*

Growing interest is paid for organic solid-state lasers (OSSLs) over the past years due to their unique features of tunability, easy processing, good flexibility, large stimulated emission cross-section, and wide-range lasing wavelength.[1] Currently, significant advances have been achieved for optically-pumped OSSLs with the improvement of their properties and advanced applications.[2] In contrast, the development of electrically-pumped OSSLs remains very challenging even it shows great potential applications in the field of organic optoelectronics due to its low-cost, comfortable and integrated device structures.

One of the main challenges for realizing electrically-driven OSSLs is the limitation of ideal organic semiconductors, which requires the integration of properties of high mobility, strong solid-state emission and lasing.[1b,3] However, it has been proved that high mobility and strong solid-state emission are mutually contradictory in one organic molecule. Therefore, it is challenging to integrate excellent optical and electronic properties in one organic semiconductor through molecular design and aggregation modulation. Currently, available high mobility organic semiconductors with highly extended π-conjugation and strong intermolecular interactions in aggregates usually exhibit very weak or even no emission, *vice versa*.[4] Besides, there will be substantial optical losses under electrical pumping associated with the contacts and multiple annihilations induced by polarons and excitons. In addition, triplet excitons formed under current injection are usually not emissive or very weak in conventional optically-pumped OSSLs due to the spin-forbidden transition from triplet excited-states to the ground state.[5] Encouragingly, some exciting advances have been made recently for the development of high mobility emissive and lasing organic semiconductors, bringing new hope for this field.[6] However, the number of lasing materials with high carrier mobility that have been reported are still very limited, and a certain quenching of luminescence efficiency is usually observed in most of them, especially in single-crystal states.[7] Single crystals have been identified as the best candidates for electrically lasing because of their intrinsically superior optoelectronic properties (high charge carrier mobility, large refractive indices, low optical loss as well as crystal giving rise to intrinsic resonators) and good stability tolerating large-density current.[4b,8] Therefore, it is urgently needed to prepare highly luminescent organic single-crystal mediums which are capable of high optical gain along with simultaneous high charge carrier mobility for electrically-stimulated lasing.

Herein, we present a high mobility organic lasing semiconductor, 2,7-diphenyl-9*H*-fluorene (LD-1, chemical structure shown in inset of Figure 1a) featuring crystallization-enhanced emission via elaborately modulating its crystal growth. Like most of currently reported high mobility emissive and lasing organic semiconductors,[6,9] to achieve the integrated electronic and optical properties, the carbon-

[*] D. Liu,[+] H. Gao, C. Gao, Z. Miao, Z. Qin, J. Yang, Prof. Dr. H. Dong
National Laboratory for Molecular Sciences, Key Laboratory of Organic Solids, Institute of Chemistry, Chinese Academy of Sciences
Beijing 100190 (China)
E-mail: dhl522@iccas.ac.cn
D. Liu,[+] Prof. Dr. Q. Peng,[+] H. Gao, Z. Miao, Z. Qin, J. Yang
University of Chinese Academy of Sciences
Beijing 100049 (China)
Prof. Dr. W. Hu
Tianjin Key Laboratory of Molecular Optoelectronic Sciences, Department of Chemistry, School of Sciences, Tianjin University&-Collaborative Innovation Center of Chemical Science and Engineering (Tianjin)
Tianjin 300072 (China)
Prof. Dr. Q. Liao,[+] J. De, Prof. Dr. H. Fu
Beijing Key Laboratory for Optical Materials and Photonic Devices, Department of Chemistry, Capital Normal University
Beijing 100048 (China)
Q. Sun, Prof. Dr. Z. Shuai
Department of Chemistry, Tsinghua University
Beijing 100084 (China)
[+] These authors contributed equally to this work.
Supporting information and the ORCID identification number(s) for the author(s) of this article can be found under: https://doi.org/10.1002/anie.202108224.

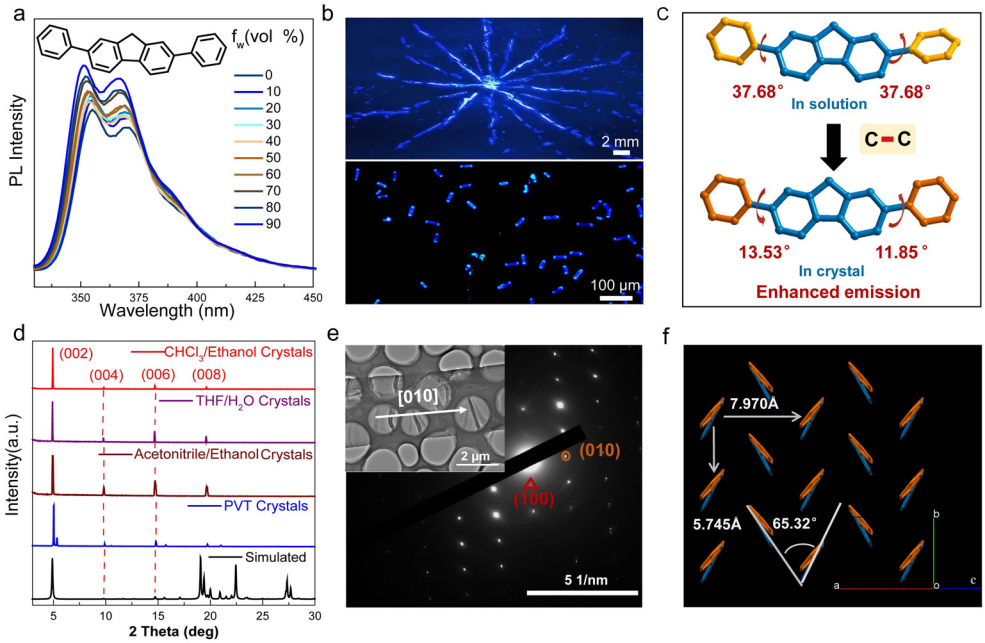

Figure 1. a) PL spectra of LD-1 ($\lambda_{ex}=320$ nm, $c=5\times10^{-6}$ M) in $CHCl_3$/ethanol mixture with adding different fractions ethanol from 0% to 90%. b) The one-dimensional nanowire crystals photographed by slow evaporation under the illumination of a UV (365 nm) lamp (top), the bottom nanowire crystals obtained by PVT under 330–380 nm light illumination. c) Molecular conformation in the diluted solution and one-dimensional nanowire crystal. d) X-ray diffraction patterns of one-dimensional nanowire crystals through different methods. e) TEM image of an individual crystal and its corresponding SAED patterns. f) The typical herringbone packing adopted of the one-dimensional nanowire single crystal.

carbon single bonds are incorporated in LD-1 compound between the π-extended benzene unit and emissive fluorene core for balanced modulation of optoelectronic properties. Such kind of molecular structure may also provide the possibility to further tune its emission property, and even enhance the luminescence efficiency by rationally tuning the molecular conformation adjusted by the twist angles of carbon-carbon single bonds and molecular conjugation.[9e] With these considerations in mind and by carrying out comprehensive investigations, we successfully obtained well-defined nanowire single crystals of LD-1, which demonstrate crystallization-enhanced photoluminescence quantum yield with a value approaching 80%. Moreover, the high carrier mobility of 0.08 $cm^2V^{-1}s^{-1}$ and superior FP lasing characters (low threshold of 86 $\mu J\,cm^{-2}$ and high-quality factor of ≈2400) were also achieved for LD-1 nanowire crystals. Thanks to its superior integrated optoelectronic properties, light-emission transistor based an individual LD-1 crystal nanowire exhibited typical electrically induced emission. This work provides a new avenue for developing high mobility lasing organic semiconductors with strong emission for electrically-pumped laser and other related ultrasmall integrated electrical-driven photonic devices.

To explore the appropriate aggregation condition of LD-1 for crystalline-enhanced emission, we carried out a systematic investigation for assembling LD-1 molecule in different solvents. Interestingly, by an intensive study, a gradually-enhanced photoluminescence emission intensity was found when poor solvent (H_2O) was added into good tetrahydrofuran (THF) solvent, or poor ethanol into trichloromethane ($CHCl_3$) and/or acetonitrile, suggesting the phenomenon of aggregation-induced emission enhancement in these conditions (Figure 1a, Figure S1).[10] More importantly, guided by these aggregation solution conditions, well-defined one-dimensional nanowire crystals of LD-1 were obtained from $CHCl_3$/ethanol, THF/H_2O and acetonitrile/ethanol mixed solutions through slow evaporation (top image of Figure 1b, Figure S2). The length of nanowire crystals is in a range of 0.5 and 2.0 mm. (Figure S3). The top image in Figure 1b shows a fluorescent flower composed of amounts of LD-1 nanowire crystals written with a brush on the substrate. Strong blue-deep emission with a PLQY value of 80% was obtained for this fluorescent flower, which shows an enhancement of around 15% PLQY compared to that of dilute solution (65%). Moreover, similar LD-1 nanowires could also be obtained by physical vapor transport (PVT) technique by modulating the growth temperature (bottom image in Figure 1b, Figure S4), demonstrating relatively small nanowire sizes and more regular crystal shapes, which are of great importance for superior optoelectronic properties in device applications. Comprehensive characterizations confirmed that all these LD-1 nanowire crystals have consistent molecular packing as evidenced by the X-ray diffraction (XRD) results and single crystal data (Figure 1c and d). It can be seen from the single crystal data that the conformation torsion angle between the benzene rotors and fluorene core in nanowire crystals is obviously reduced from around 38° in solution to 12–14° in crystal. These results suggest that the LD-1 molecular structure is more rigid in nanowire crystals, which in principle is beneficial for higher photoluminescence emission due to the enhancement of radiation transition rate.[11] Figure 1e shows the transmission electron microscopy (TEM) image and its corresponding selected area electron diffraction (SAED) patterns. The diffraction peaks could be well indexed according to the single crystal data (Table S1, Figure S5).[12] The spots marked by the red triangle and yellow circle were ascribed to the (100) and (010) crystal planes, respectively by comparing the calculated interplanar distance with $d_{(100)}=8.20$ Å and $d_{(010)}=5.85$ Å, respectively. This proves that LD-1 nanowires grow along the [010] direction, which is corresponding to the strong molecular packing direction in the herringbone structure, as shown in Figure 1f. This direction is also the beneficial charge transport direction

in the following constructed electronic and electroluminescent devices.

To deeply investigate the photoluminescence enhancement mechanism of LD-1 nanowires, we performed further detailed photophysical studies experimentally and theoretically. Compared to that of LD-1 in solution, an obvious red-shift photoluminescence emission with the strongest peak from 397 nm to 409 nm was observed (Figure S6a), which is consistent with the extended molecular conjugation. The time-resolved peak fluorescence was also accomplished (Figure S6b). According to the $k_r = \Phi_F/\tau_{ave}$ equation, the calculated radiative decay rate ($k_r = 4.26 \times 10^8\ s^{-1}$) of nanowire crystals is enhanced, while the non-radiative deactivation rate (k_{nr}) is reduced compared to that of LD-1 in solution,[6d] suggesting the potential emission enhancement for LD-1 nanowires. More deep theoretical calculation further confirmed this point. As shown in Figure 2a, it can be seen that the largest contributions to the reorganization energy from one low frequency mode and several high frequency modes in solution. Their frequencies and reorganization energies are 47.09 cm^{-1}/429.41 cm^{-1}, 1693 cm^{-1}/301.26 cm^{-1}, and 1701.37 cm^{-1}/1054.41 cm^{-1}, respectively. In contrast, there are three dominant high frequency modes (1334.65 cm^{-1}/225.07 cm^{-1}, 1698.55 cm^{-1}/459.38 cm^{-1}, and 1709.29 cm^{-1}/443.65 cm^{-1}) in nanowire crystals. The decrease of total reorganization energy from 433 meV to 378 meV in crystal is caused by the restriction of rotational, stretching vibrations, and twisting from the displacement vectors, which leads to the reduction of the non-radiative rate as indicated in Figure 2b. And it is well consistent with that of experimental values. Moreover, the 0–0 band transition is very weak in solution and it only manifests the 0–1 transition of mode 3 ($\omega = 52.48\ cm^{-1}$), 4 ($\omega = 62.43\ cm^{-1}$), 88 ($\omega = 1382.94\ cm^{-1}$), 103 ($\omega = 1701.37\ cm^{-1}$) and 0–8 transition of mode 2 ($\omega = 47.09\ cm^{-1}$), which suggests that exciton coupling show little effect on the efficiency of luminescence (Figure S7). The emission enhancement of LD-1 nanowire crystals is mainly attributed to the extended π-conjugation of molecules with the reduction of non-radiative rate and weak exciton coupling effect. Figure 2c shows a well-separated four-energy level required by population inversion in crystals. The photon is pumped to the first singlet excited state S_1 ($v_e = 1$) from the ground state S_0 ($v_g = 0$). Then, the molecule will loosen rapidly to the S_1 ($v_e = 0$). Population inversion and the lasing action can be easily realized at the $v_e = 0$ and $v_g = 1$ states. And a large emission oscillator strength (f_{em}) of 1.66, high PLQY, quick k_r make LD-1 nanowire crystals have the potential to serve as a good optical gain medium for lasing.[5a]

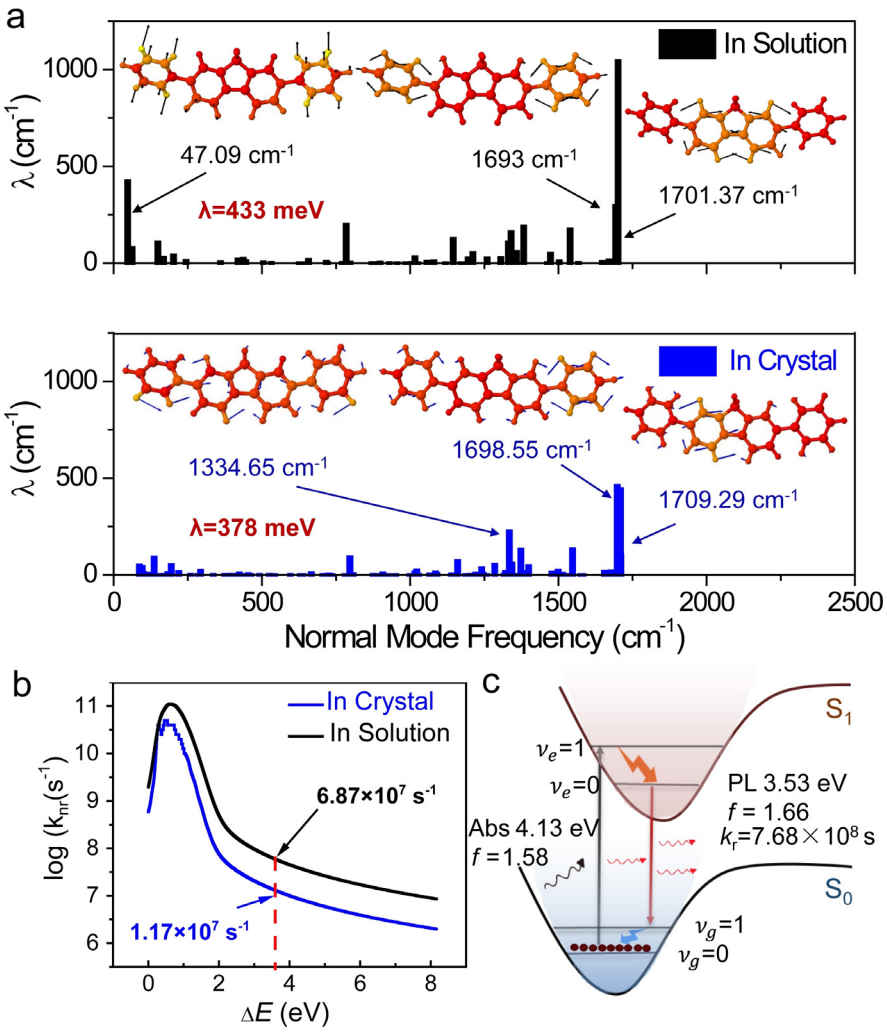

Figure 2. a) Reorganization energy (λ) based on the potential surface in solution and crystal, as well as their contributed vibration modes. b) Calculated non-radiative rate *vs* energy difference ΔE in solution and crystal. c) Organic four-level system with vertical vibronic transitions energy and corresponding oscillator strength.

In addition, amplified spontaneous emission (ASE) and lasing characters of LD-1 crystals were further studied. As shown in Figure S8, the ASE spectra exhibit typical optical amplification at peaks of 394 nm and 407 nm with the threshold energy density of 806 μJ cm^{-2} and 803 μJ cm^{-2}, respectively. Besides, the optical gain of 30 cm^{-1} and the loss of 10.6 cm^{-1} were also demonstrated for such crystals. Figure 3a displays the high-resolution PL spectra of an individual LD-1 nanowire crystal evolved as a function of excitation pulse energy. When the pump density exceeds the lasing threshold, a series of sharp peaks on the broad spontaneous spectrum were observed with the spectral peak centered at about 390 nm, indicating the generation of lasing characteristic. As plotted in Figure 3b, the PL peak intensity increased nonlinearly above lasing threshold (E_{th}) of 86 μJ cm^{-2}, which is identified as the excitation density

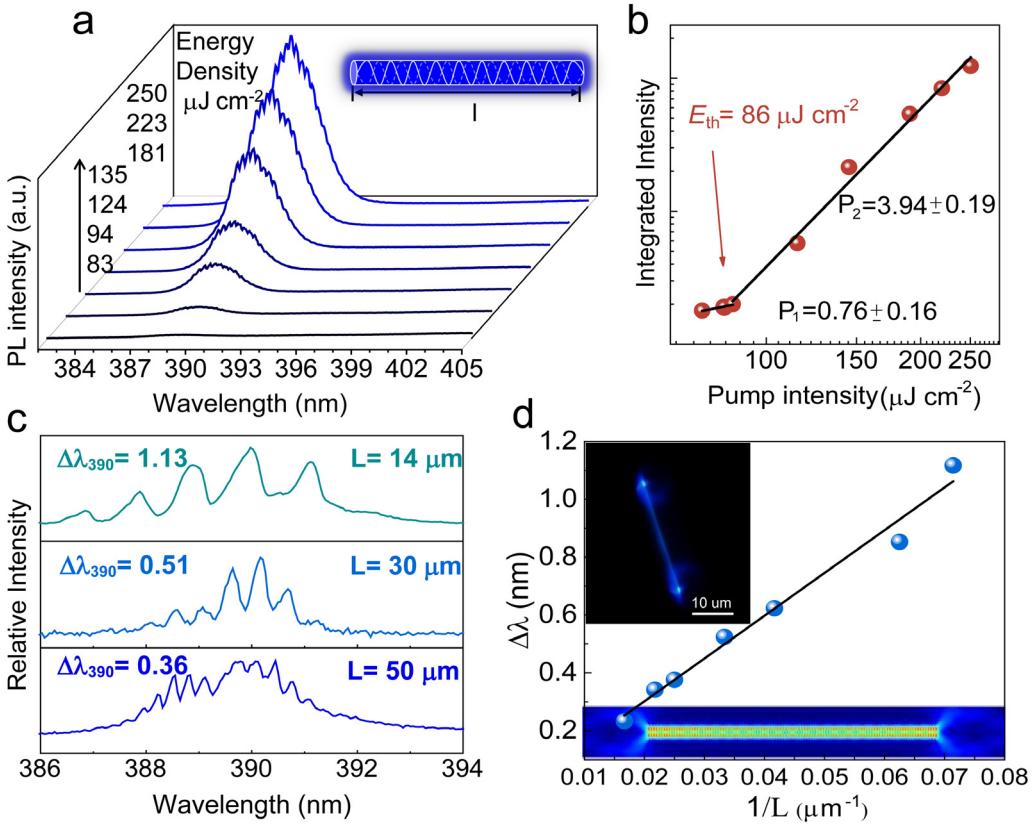

Figure 3. a) High-resolution PL spectrums of the one-dimensional nanowire crystal under different pump densities at 390 nm. Inset: illustrate a typical optical-ray analysis within FP microcavity. b) PL integrated area of the 390 nm as a function of pump density for a one-dimensional nanowire crystal. c) The laser spectra of three different lengths for one-dimensional nanowire crystals above the threshold. d) The mode spacing $\Delta\lambda$ relationship with the 1/L of the one-dimensional nanowire crystals. Inset: Two strong deep-blue impressive spots at both one-dimensional nanowire crystal ends. And optical mode simulation result for a one-dimensional nanowire crystal with L = 15 μm (λ = 390 nm), Q = 2212.

along with the behavior changing. Meanwhile, two strong deep-blue impressive spots at the ends of a single nanowire are also observed (inset of Figure 3 d), which is a peculiarity of Fabry-Perot (FP) optical micro-resonator comprising two parallel facets of the nanowire crystal sides for lasing.

As shown in Figure 3 c, the association between the mode spacing ($\Delta\lambda$) and optical path length (L = 2l) of LD-1 nanowire crystal was further described by $\Delta\lambda = \lambda^2/(L[n-\lambda(dn/d\lambda)])$, where λ is the light of wavelength, $[n-\lambda(dn/d\lambda)]$ is the group refractive index.[2a,13] For instance, $\Delta\lambda_{390} = 1.13$, 0.51, and 0.36 nm for length L = 14, 30, and 50 μm, respectively. The $\Delta\lambda$ gradually decreases and reveals more modes with the increase of the L. A plot of 1/L versus the $\Delta\lambda$ (Figure 3 d). It is noticed that the best-fit line (black line) is linear, which verifies that (FP) resonator along the nanowire direction. Additionally, the simulation of 2D electric field distribution of the nanowire crystal along the cross-section verifies that the FP resonator with the high-quality factor (Q) of 2212. This simulated result is also consistent with the high experimental Q value of 2400 according to the following expression: $Q = \lambda/\Delta\lambda_L$, where λ is the lasing peak of 390 nm, $\Delta\lambda_L$ is a full-width at half maximum (FWHM) of the lasing peak of 0.16 nm.[14]

According to the atomic force microscope (AFM) measurement, the crystal thickness is ≈400 nm with a smooth surface, demonstrating the high-quality of micro/nanometer-sized crystals (Figure S9). To investigate the charge transport property, we further fabricated an organic field-effect transistor (OFET) based on an individual LD-1 nanowire crystal (Figure S10). Efficient charge transport with carrier mobility of around 0.08 $cm^2 V^{-1} s^{-1}$ was obtained along the long axis of nanowire according to the transfer curves of LD-1-based OFETs (Figure S11), which is the tight molecular packing direction in crystal (as shown in Figure 1 f). All the above results demonstrate that LD-1 nanowire crystals are superior high mobility lasing organic semiconductors with strong emission. So that, OLETs were successfully constructed based on an individual LD-1 nanowire (Figure 4 a). OLET is an ideal device platform for the exploration of electrically-pumped organic lasers due to its intrinsic current amplification characteristic under the gate modulation as well as the possibility of reducing the optical losses and achieving much higher efficiency in such a lateral device configuration.[15] For LD-1 based OLET, to ensure efficient holes and electrons simultaneously inject into the conducting channel for radical recombination emission, an asymmetric OLET device geometry was conducted with the low-work function electrode of Al/Cs_2CO_3 for electron injection and high-work function electrode of Au/MoO_3 for hole injection, respectively (Figure 4 b). Under the modulation of source-drain and gate voltages, typical electrically-driven emission was obtained within the LD-1 nanowire (Figure 4 c and Figure S12). The electroluminescence spectrum of LD-1-based OLET is also

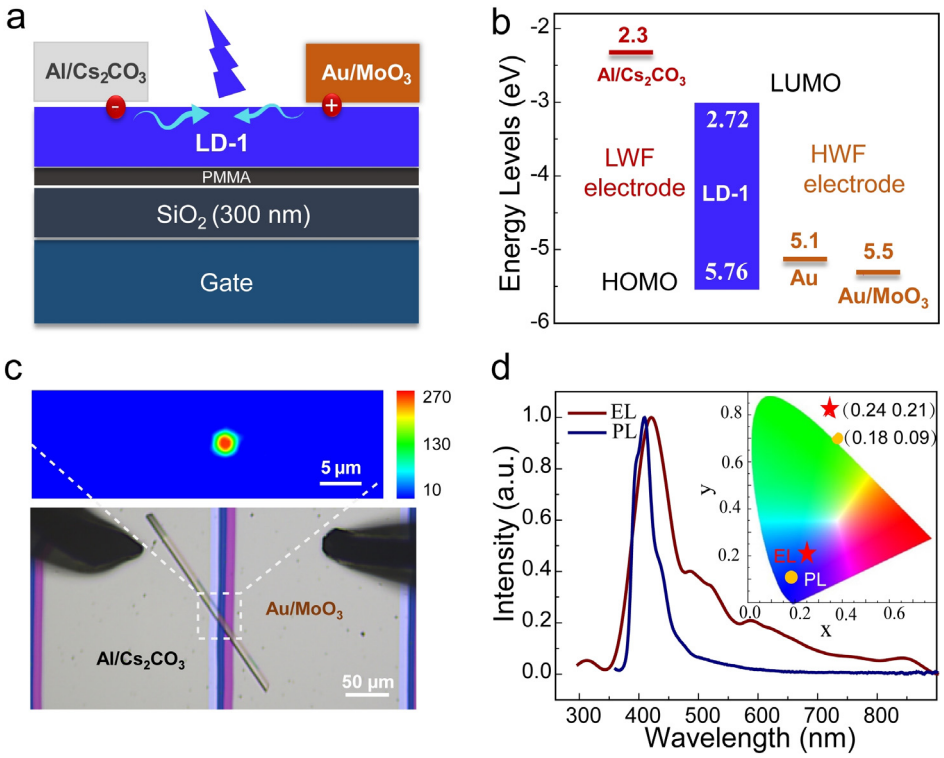

Figure 4. a) One-dimensional nanowire single crystal-based OLETs. b) Energy levels of Al/Cs_2CO_3, LD-1 and Au/MoO_3 in a single crystal OLET device. c) Optical image of a typical one-dimensional nanowire of the OLET device. Color-coded image for a one-dimensional nanowire single crystal-based OLET extracted from light emission captured by CCD camera. d) EL, PL spectra and their corresponding CIE 1931 coordinates of one-dimensional nanowire single crystal-based OLET, and the EL curve was slightly smoothed.

well-identical with that of photoluminescence spectrum with the strongest peak at around 421 nm (Figure 4d), which is a kind of unique deep-blue emission.[16] Such kind of LD-1 nanowire-OLET provides a good platform for potential study of electrically pumped organic lasers and other related ultrasmall integrated electrical-driven photonic devices.[17]

In conclusion, a kind of high mobility organic laser semiconductor of LD-1 with strong emission in its nanowire crystals is demonstrated by carefully modulating its molecule aggregation conditions. Comprehensive experimental and theoretical results confirm that LD-1 nanowire crystals possess a very high PLQY value approaching 80%, efficient charge carrier mobility and superior FP lasing characters. Combined these good optoelectronic properties, OLET based on an individual LD-1 nanowire crystal was successfully constructed, which gives typical electrically-driven deep-blue emission due to the recombination of holes and electrons simultaneously injected into the nanowire. Such research concept could be extended to other π-conjugated organic molecules for superior integrated optoelectronic properties. In addition, this work also provides a new avenue for developing high-performance organic laser semiconductors and other related ultrasmall integrated electrical-driven photonic devices.

Acknowledgements

This work was supported by the Ministry of Science and Technology of China (2017YFA0204503, 2018YFA0703200), the National Natural Science Foundation of China (Grant No.51725304, 22021002, 61890943, 91833306), Beijing National Laboratory for Molecular Sciences (BNLMS-CXXM-202012), the International Cooperation Program of Chinese Academy of Sciences (GJTD-2020-02, 121111KYSB20200004) and the Youth Innovation Promotion Association of the Chinese Academy of Sciences.

Conflict of Interest

The authors declare no conflict of interest.

Keywords: crystallization-enhanced emission · high mobility · lasing character · OLET

[1] a) A. J. C. Kuehne, M. C. Gather, *Chem. Rev.* **2016**, *116*, 12823–12864; b) I. D. Samuel, G. A. Turnbull, *Chem. Rev.* **2007**, *107*, 1272–1295; c) R. F. Service, *Science* **2010**, *328*, 810–811; d) S. Kéna-Cohen, S. R. Forrest, *Nat. Photonics* **2010**, *4*, 371–375.

[2] a) X. Wang, Q. Liao, Q. Kong, Y. Zhang, Z. Xu, X. Lu, H. Fu, *Angew. Chem. Int. Ed.* **2014**, *53*, 5863–5867; *Angew. Chem.* **2014**, *126*, 5973–5977; b) H. Fang, Q. Chen, J. Yang, H. Xia, B. Gao, J. Feng, Y. Ma, H. Sun, *J. Phys. Chem. C* **2010**, *114*, 11958–11961; c) Z. Yu, Y. Wu, Q. Liao, H. Zhang, S. Bai, H. Li, Z. Xu, C. Sun, X. Wang, J. Yao, H. Fu, *J. Am. Chem. Soc.* **2015**, *137*, 15105–15111; d) K. Wang, Z. Gao, W. Zhang, Y. Yan, H. Song, X. Lin, Z. Zhou, H. Meng, A. Xia, J. Yao, Y. Zhao, *Sci. Adv.* **2019**, *5*, eaaw2953.

[3] a) N. Tessler, *Adv. Mater.* **1999**, *11*, 363–370; b) S. A. Jenekhe, *Nat. Mater.* **2008**, *7*, 354–355.

[4] a) T. M. Figueira-Duarte, K. Müllen, *Chem. Rev.* **2011**, *111*, 7260–7314; b) X. Zhang, H. Dong, W. Hu, *Adv. Mater.* **2018**, *30*, 1801048; c) Y. G. Ma, J. C. Shen, *Sci. China Ser. B* **2007**, *37*, 105–123; d) J. Yang, D. Yan, T. S. Jones, *Chem. Rev.* **2015**, *115*, 5570–5603; e) D. Ma, G. Wang, Y. Hu, Y. Zhang, L. Wang, X. Jing, F. Wang, C. S. Lee, S. T. Lee, *Appl. Phys. Lett.* **2003**, *82*, 1296.

[5] a) Q. Ou, Q. Peng, Z. Shuai, *Nat. Commun.* **2020**, *11*, 4485; b) M. Baldo, R. Holmes, S. Forrest, *Phys. Rev. B* **2002**, *66*, 035321; c) A. S. D. Sandanayaka, L. Zhao, D. Pitrat, J. C. Mulatier, T. Matsushima, C. Andraud, J. H. Kim, J. C. Ribierre, C. Adachi, *Appl. Phys. Lett.* **2016**, *108*, 223301; d) K. Hayashi, H. Nakanotani, M. Inoue, K. Yoshida, O. Mikhnenko, T. Q. Nguyen, C. Adachi, *Appl. Phys. Lett.* **2015**, *106*, 093301.

[6] a) B. K. Yap, R. Xia, M. C. Quiles, P. N. Stavrinou, D. D. C. Bradley, *Nat. Mater.* **2008**, *7*, 376–380; b) K. Nakamura, M. Ichikawa, R. Fushiki, T. Kamikawa, M. Inoue, T. Koyama, Y.

Taniguchi, *Jpn. J. Appl. Phys.* **2005**, *44*, L1367 – L1369; c) M. Ichikawa, K. Nakamura, M. Inoue, H. Mishima, T. Haritani, R. Hibino, T. Koyama, Y. Taniguchi, *Appl. Phys. Lett.* **2005**, *87*, 221113; d) D. Liu, J. De, H. Gao, S. Ma, Q. Ou, S. Li, Z. Qin, H. Dong, Q. Liao, B. Xu, Q. Peng, Z. Shuai, W. Tian, H. Fu, X. Zhang, Y. Zhen, W. Hu, *J. Am. Chem. Soc.* **2020**, *142*, 6332 – 6339; e) S. Ma, K. Zhou, M. Hu, Q. Li, Y. Liu, H. Zhang, J. Jing, H. Dong, B. Xu, W. Hu, W. Tian, *Adv. Funct. Mater.* **2018**, *28*, 1802454; f) J. Deng, Y. Xu, L. Liu, C. Feng, J. Tang, Y. Gao, Y. Wang, B. Yang, P. Lu, W. Yang, Y. Ma, *Chem. Commun.* **2016**, *52*, 2647 – 2647; g) X. Yu, T. J. Marks, A. Facchetti, *Nat. Mater.* **2016**, *15*, 383 – 396; h) J. Zhang, S. Ma, H. Fang, B. Xu, H. Sun, I. Chancd, W. Tian, *Mater. Chem. Front.* **2017**, *1*, 1422 – 1429; i) G. Shan, X. Li, W. Huang, *The Innovation* **2020**, *1*, 100031; j) W. Zhu, A. P. Spencer, S. Mukherjee, J. M. Alzola, V. K. Sangwan, S. H. Amsterdam, S. M. Swick, L. O. Jones, M. C. Heiber, A. A. Herzing, G. Li, C. L. Stern, D. M. DeLongchamp, K. L. Kohlstedt, M. C. Hersam, G. C. Schatz, M. R. Wasielewski, L. X. Chen, A. Facchetti, T. J. Marks, *J. Am. Chem. Soc.* **2020**, *142*, 14532 – 14547; k) Z. Wang, Y. Zou, W. Chen, Y. Huang, C. Yao, Q. Zhang, *Adv. Electron. Mater.* **2019**, *5*, 1800547; l) A. Shukla, V. T. N. Mai, A. M. C. Senevirathne, I. Allison, S. K. M. McGregor, R. J. Lepage, M. Wood, T. Matsushima, E. G. Moore, E. H. Krenske, A. S. D. Sandanayaka, C. Adachi, E. B. Namdas, S.-C. Lo, *Adv. Opt. Mater.* **2020**, *8*, 2000784; m) J. Yang, Q. Liu, M. Hu, S. Ding, J. Liu, Y. Wang, D. Liu, H. Gao, W. Hu, H. Dong, *Sci. China Chem.* **2021**, https://doi.org/10.1007/s11426-021-1037-3; n) Y. Liu, Y. Guo, Y. Liu, *Small Struct.* **2021**, *2*, 2000083; o) S. Ma, S. Du, G. Pan, S. Dai, B. Xu, W. Tian, *Aggregate* **2021**, *61*, e96.

[7] a) A. Dadvand, W. Sun, A. Moiseev, F. Belanger-Gariepy, F. Rosei, H. Meng, D. Perepichka, *J. Mater. Chem. C* **2013**, *1*, 2817 – 2825; b) J. Liu, W. Zhu, K. Zhou, Z. Wang, Y. Zou, Q. Meng, J. Li, Y. Zhen, W. Hu, *J. Mater. Chem. C* **2016**, *4*, 3621 – 3627; c) M. Chen, Y. Zhao, L. Yan, S. Yang, Y. Zhu, I. Murtaza, G. He, H. Meng, W. Huang, *Angew. Chem. Int. Ed.* **2017**, *56*, 722 – 727; *Angew. Chem.* **2017**, *129*, 740 – 745; d) C. Wang, Y. Liu, Z. Wei, H. Li, W. Xu, W. Hu, *Appl. Phys. Lett.* **2010**, *96*, 143302; e) J. Liu, L. Meng, W. Zhu, C. Zhang, H. Zhang, Y. Yao, Z. Wang, P. He, X. Zhang, Y. Wang, Y. Zhen, H. Dong, Y. Yi, W. Hu, *J. Mater. Chem. C* **2015**, *3*, 3068 – 3071; f) J. Liu, J. Liu, Z. Zhang, C. Xu, Q. Li, K. Zhou, H. Dong, X. Zhang, W. Hu, *J. Mater. Chem. C* **2017**, *5*, 2519 – 2523; g) A. Dadvand, A. Moiseev, K. Sawabe, W. Sun, B. Djukic, I. Chung, T. Takenobu, F. Rosei, D. Perepichka, *Angew. Chem. Int. Ed.* **2012**, *51*, 3837 – 3841; *Angew. Chem.* **2012**, *124*, 3903 – 3907; h) H. Ju, K. Wang, J. Zhang, H. Geng, Z. Liu, G. Zhang, Y. Zhao, D. Zhang, *Chem. Mater.* **2017**, *29*, 3580 – 3588.

[8] a) C. Wang, H. Dong, L. Jiang, W. Hu, *Chem. Soc. Rev.* **2018**, *47*, 422 – 500; b) J. Wu, Q. Li, G. Xue, H. Chen, H. Li, *Adv. Mater.* **2017**, *29*, 1606101; c) H. Jiang, P. Hu, J. Ye, R. Ganguly, Y. Li, Y. Long, D. Fichou, W. Hu, C. Kloc, *Angew. Chem. Int. Ed.* **2018**, *57*, 10112 – 10117; *Angew. Chem.* **2018**, *130*, 10269 – 10273; d) F. Yang, L. Sun, Q. Duan, H. Dong, Z. Jing, Y. Yang, R. Li, X. Zhang, W. Hu, L. Chua, *SmartMat* **2021**, *2*, 99 – 108; e) Y. Zhen, H. Dong, L. Jiang, W. Hu, *Chin. Chem. Lett.* **2016**, *27*, 1330 – 1338; f) G. Zhao, H. Dong, Q. Liao, J. Jiang, Y. Luo, H. Fu, W. Hu, *Nat. Commun.* **2018**, *9*, 4790; g) M. Hu, J. Liu, Q. Zhao, D. Liu, Q. Zhang, K. Zhou, J. Li, H. Dong, W. Hu, *Sci. China Mater.* **2019**, *62*, 729 – 735; h) C. Wang, J. Zhang, G. Long, N. Aratani, H. Yamada, Y. Zhao, Q. Zhang, *Angew. Chem. Int. Ed.* **2015**, *54*, 6292 – 6296; *Angew. Chem.* **2015**, *127*, 6390 – 6394; i) J. Tao, D. Liu, Z. Qin, B. Shao, J. Jing, H. Li, H. Dong, B. Xu, W. Tian, *Adv. Mater.* **2020**, *32*, 1907791.

[9] a) J. Liu, H. Zhang, H. Dong, L. Meng, L. Jiang, L. Jiang, Y. Wang, J. Yu, Y. Sun, W. Hu, *Nat. Commun.* **2015**, *6*, 10032; b) J. Li, K. Zhou, J. Liu, Y. Zhen, L. Liu, J. Zhang, H. Dong, X. Zhang, L. Jiang, W. Hu, *J. Am. Chem. Soc.* **2017**, *139*, 17261 – 17264; c) Z. Qin, H. Gao, J. Liu, K. Zhou, J. Li, Y. Dang, L. Huang, H. Deng, X. Zhang, H. Dong, W. Hu, *Adv. Mater.* **2019**, *31*, 1903175; d) D. Liu, J. Li, J. Liu, X. Lu, M. Hu, Y. Li, Z. Shu, Z. Ni, S. Ding, L. Jiang, Y. Zhen, X. Zhang, H. Dong, W. Hu, *J. Mater. Chem. C* **2018**, *6*, 3856 – 3860; e) Z. Xie, D. Liu, Y. Zhang, Q. Liu, H. Dong, W. Hu, *Chem. J. Chin. Univ.* **2020**, *41*, 1179 – 1193; f) X. Guo, Y. Zhang, Y. Hu, J. Yang, Y. Li, Z. Ni, H. Dong, W. Hu, *Angew. Chem. Int. Ed.* **2021**, *60*, 14902 – 14908; *Angew. Chem.* **2021**, *133*, 15028 – 15034; g) Q. Liu, Y. Zhang, C. Gao, T. Wang, W. Hu, H. Dong, *Acta Chim. Sin.* **2020**, *78*, 945 – 953; h) Y. Zhang, J. Ye, Z. Liu, Q. Liu, X. Guo, Y. Dang, J. Zhang, Z. Wei, Z. Wang, Z. Wang, H. Dong, W. Hu, *J. Mater. Chem. C* **2020**, *8*, 10868 – 10879; i) Y. Yao, Y. Chen, H. Wang, P. Samorì, *SmartMat* **2020**, *1*, e1009.

[10] a) R. Deans, J. Kim, M. R. Machacek, T. M. Swager, *J. Am. Chem. Soc.* **2000**, *122*, 8565 – 8566; b) Q. Zeng, Z. Li, Y. Dong, C. Di, A. Qin, Y. Hong, L. Ji, Z. Zhu, C. K. W. Jim, G. Yu, Q. Li, Z. Li, Y. Liu, J. Qin, B. Z. Tang, *Chem. Commun.* **2007**, 70 – 72; c) B. K. An, S. K. Kwon, S. D. Jung, S. Y. Park, *J. Am. Chem. Soc.* **2002**, *124*, 14410 – 14415; d) L. Xu, Z. Wang, R. Wang, L. Wang, X. He, H. Jiang, H. Tang, D. Cao, B. Z. Tang, *Angew. Chem. Int. Ed.* **2020**, *59*, 9908 – 9913; *Angew. Chem.* **2020**, *132*, 9994 – 9999; e) D. Liu, M. Chen, K. Li, Z. Li, J. Huang, J. Wang, Z. Jiang, Z. Zhang, T. Xie, G. R. Newkome, P. Wang, *J. Am. Chem. Soc.* **2020**, *142*, 7987 – 7994; f) J. Li, J. Wang, H. Li, N. Song, D. Wang, B. Z. Tang, *Chem. Soc. Rev.* **2020**, *49*, 1144 – 1172.

[11] a) J. Luo, Z. Xie, J. W. Y. Lam, L. Cheng, H. Chen, C. Qiu, H. S. Kwok, X. Zhan, Y. Liu, D. Zhu, B. Z. Tang, *Chem. Commun.* **2001**, 1740 – 1741; b) J. Mei, N. L. Leung, R. T. Kwok, J. W. Lam, B. Z. Tang, *Chem. Rev.* **2015**, *115*, 11718 – 11940; c) H. Wang, E. Zhao, J. W. Y. Lam, B. Z. Tang, *Mater. Today* **2015**, *18*, 365 – 377; d) Z. Zhao, H. Zhang, J. W. Y. Lam, B. Tang, *Angew. Chem. Int. Ed.* **2020**, *59*, 9888 – 9907; *Angew. Chem.* **2020**, *132*, 9972 – 9993.

[12] Deposition Number 1942285 contains the supplementary crystallographic data for this paper. These data are provided free of charge by the joint Cambridge Crystallographic Data Centre and Fachinformationszentrum Karlsruhe Access Structures service www.ccdc.cam.ac.uk/structures.

[13] a) Z. Xu, Q. Liao, Q. Shi, H. Zhang, J. Yao, H. Fu, *Adv. Mater.* **2012**, *24*, 216 – 220; b) Y. Zhao, A. Peng, H. Fu, Y. Ma, J. Yao, *Adv. Mater.* **2008**, *20*, 1661 – 1665.

[14] a) H. Dong, C. Zhang, Y. Liu, Y. Yan, F. Hu, Y. S. Zhao, *Angew. Chem. Int. Ed.* **2018**, *57*, 3108 – 3112; *Angew. Chem.* **2018**, *130*, 3162 – 3166; b) C. Ou, X. Ding, Y. Li, C. Zhu, M. Yu, L. Xie, J. Lin, C. Xu, W. Huang, *J. Phys. Chem. C* **2017**, *121*, 14803 – 14810.

[15] a) S. Z. Bisri, T. Takenobub, Y. Iwasacd, *J. Mater. Chem. C* **2014**, *2*, 2827 – 2836; b) Z. Qin, H. Gao, H. Dong, W. Hu, *Adv. Mater.* **2021**, *33*, 2007149; c) L. Hou, X. Zhang, G. F. Cotella, G. Carnicella, M. Herder, B. M. Schmidt, M. Pätzel, S. Hecht, F. Cacialli, P. Samorì, *Nat. Nanotechnol.* **2019**, *14*, 347 – 353; d) M. Ullah, K. Tandy, S. D. Yambem, M. Aljada, P. L. Burn, P. Meredith, E. B. Namdas, *Adv. Mater.* **2013**, *25*, 6213 – 6218.

[16] a) Y. H. Kim, D. C. Shin, S. H. Kim, C. H. Ko, H. S. Yu, Y. S. Chae, S. K. Kwon, *Adv. Mater.* **2001**, *13*, 1690 – 1693; b) Z. Gao, Z. Li, P. Xia, M. Wong, K. W. Cheah, C. H. Chen, *Adv. Funct. Mater.* **2007**, *17*, 3194 – 3199.

[17] a) P. B. W. Jensen, J. Kjelstrup-Hansen, H. G. Rubahn, *Org. Electron.* **2013**, *14*, 3324 – 3330; b) D. Tu, S. Pagliara, A. Camposeo, L. Persano, R. Cingolaniac, D. Pisignano, *Nanoscale* **2010**, *2*, 2217 – 2222; c) J. H. Kim, A. Watanabe, J. W. Chung, Y. Jung, B. K. An, H. Tada, S. Y. Park, *J. Mater. Chem.* **2010**, *20*, 1062 – 1064; d) E. Orgiu, P. Samorì, *Adv. Mater.* **2014**, *26*, 1827 – 1845.

Manuscript received: June 21, 2021
Accepted manuscript online: July 18, 2021
Version of record online: August 11, 2021

